

The secular evolution of planetary nebula IC 418 and its implications for carbon star formation

ALBERT A. ZIJLSTRA¹ AND QUENTIN A. PARKER²

¹*Jodrell Bank Centre for Astrophysics, Department of Physics and Astronomy
The University of Manchester, Oxford Road, M13 9PL, Manchester, UK*

²*The Laboratory for Space Research, Faculty of Science,
The University of Hong Kong, Cyberport 4, Hong Kong*

ABSTRACT

The rate of stellar evolution can rarely be measured in real time. The fastest evolution (excluding event-driven evolution), where stars may evolve measurably over decades, is during the post-AGB phase. In this paper we provide direct evidence for such a case. A secular, linear, factor of ~ 2.5 increase is found in the strength of the [O III] lines relative to $H\beta$ over an 130 year period in the young, well-known, low excitation planetary nebula IC 418. The increase is caused by the rising temperature of the central star. We use photo-ionization models to derive a model dependent heating rate for the central star in the range $15\text{--}42\text{ K yr}^{-1}$. These derived heating rates are very sensitive to the stellar mass, and yield a central-star mass of $\sim 0.560\text{--}0.583\text{ M}_{\odot}$. Initial-final mass relations based on the Miller-Bertolami models give a progenitor main-sequence mass of $1.25\text{--}1.55\text{ M}_{\odot}$. IC 418 is a carbon rich planetary nebula and its central star, HD 35914, has evolved from an AGB carbon star. This result shows that carbon star formation at solar metallicity extends to these low masses. This is lower than commonly assumed and suggests that post-AGB evolution may be slower than recent post-AGB models predict.

Keywords: ISM: planetary nebulae: stars – evolution – techniques: photometric – techniques: spectroscopic

1. INTRODUCTION

Planetary nebulae (PNe) are a short-lived phase in the late evolution of low to intermediate-mass stars (K. B. Kwitter & R. B. C. Henry 2022), after the star has terminated the Asymptotic Giant Branch (AGB) phase. On the AGB, the progenitor star loses 40% to 80% of its mass (S. Höfner & H. Olofsson 2018) over several hundred thousand years via pulsations and dust-driven winds. The remnant proto-white-dwarf core heats up to temperatures $T \sim 10^5\text{ K}$ before nuclear burning ceases. Thereafter, the stellar luminosity rapidly drops as the stellar core contracts and enters the white dwarf (WD) cooling track. The expanding nebula from the ejected envelope becomes ionized once the residual central star (CSPN) reaches $T = 20\text{--}25\text{ kK}$. The onset of Balmer line emission signals the brief PN phase which typically lasts for 5,000 to 25,000 years (e.g., A. Ali et al. 2015).

Ionisation increases with CSPN temperature evolution during the PN phase. Between an CSPN T_{eff} of 30 and 45 kK the integrated [O III] and [Ne III] emission increase by more than an order of magnitude, while the integrated, higher excitation He II emission strongly increases between 60 and 80 kK. The rate of CSPN temperature increase is a very strong function of stellar mass (T. Bloeker 1995). This can give significant evolution on decadal timescales detectable photometrically and spectroscopically. If accurate spectrophotometry over several decades exists, such changes can be observed and quantified (M. Hajduk et al. 2015). This is a powerful technique, since if the CSPN heating rate can be measured, the CSPN mass can be inferred to much higher accuracy than is possible from its luminosity (K. Gesicki & A. A. Zijlstra 2007; T. Bloeker 1995). With the current mass and using the initial-final mass relation, e.g. J. D. Cummings et al. (2018), the progenitor star’s mass and age can be derived, yielding key information on stellar evolution.

The CSPN fades optically because most of its energy is increasingly emitted at shorter wavelengths as the star heats up on its way to becoming a WD. Secular changes in the star’s visual magnitude are expected to be small on decadal timescales, whereas spectroscopic changes in the nebula can be more pronounced and easier to detect.

PNe spectroscopy is 150+ years old (W. Huggins & W. A. Miller 1864), so uncovering evolution is possible if sufficient observations for suitable PNe exist. However, very few PNe have decent spectral coverage, repeated over time periods sufficient to reveal secular evolution of their CSPN. The young, high surface brightness PN IC 418 is one such rare example with a long, 130 year record of spectroscopic observation as one of the first PN identified. Furthermore, it is in a low ionisation state where CSPN evolution over relatively short timescales is easier to discern. This makes IC 418 uniquely suitable for studying real-time spectroscopic evolution of a PN.

Here, we present strong observational evidence for a significant factor ~ 2.5 increase in the observed $[\text{O III}]\lambda 5007/\text{H}\beta$ ratio in this bright PN as revealed by carefully vetting, and in some cases re-measuring, diverse, archival, spectroscopic data available over 130 years, and including our own more recent observations.³

1.1. PNe with evidence for evolution

The few PNe that have coverage over sufficient time to reveal secular evolution include NGC 7027 (A. A. Zijlstra et al. 2008, from radio flux measurements), Hen 2-260 (M. Hajduk et al. 2014), NGC 6572 (V. P. Arkhipova et al. 2014) and IC 4997 (L. H. Aller & W. Liller 1966; W. A. Feibelman et al. 1992; E. B. Kostyakova & V. P. Arkhipova 2009) (all from spectroscopy). NGC 6572 in particular has evidence of an increase in the observed $[\text{O III}]/\text{H}\beta$ ratio between 1938 and 2013 by as much as $\sim 30\%$. Two additional $[\text{O III}]/\text{H}\beta$ data points (T. Barker 1979; R. Bandyopadhyay et al. 2023) that were not in V. P. Arkhipova et al. (2014) confirm this mild evolution from what is already a high $[\text{O III}]/\text{H}\beta$ ratio of ~ 10 .

Several other candidates with 50-60 year observational baselines were noted by M. Hajduk et al. (2015) including M 1-11, M 1-12, M 1-26, H 2-48 and H 2-25 but these require more detailed investigation.

There is more evidence for flux changes in cooler post-AGB stars (pre-PNe), where variations are seen in Hen 3-1357 (N. Reindl et al. 2017), CRL 618 (C. Sánchez Contreras et al. 2017) and IRAS 18062+2410 (L. Cerrigone et al. 2017) but with some uncertainty whether this is secular evolution, event-driven evolution (e.g., post-thermal-pulse or common envelope) or variability.

2. THE PLANETARY NEBULA IC 418

IC 418 (informally known as the Spirograph Nebula), is a well-known, high-surface brightness, compact, mildly elliptical PN in the constellation of Lepus. It measures $14'' \times 12''$ across (D. J. Frew et al. 2016). Two concentric but very faint ionized optical halos are better seen in the mid-infrared (G. Ramos-Larios et al. 2012). The ionized region has an estimated mass of $0.06 M_{\odot}$ (C. Morisset & L. Georgiev 2009). A photo-dominated region (PDR) with an estimated mass of $\sim 0.5 M_{\odot}$ contains neutral hydrogen (A. R. Taylor et al. 1989) and other atomic lines (X.-W. Liu et al. 2001). A dusty, molecular region shows carbonaceous dust, including PAHs and weak fullerene bands (M. Otsuka et al. 2014; J. J. Díaz-Luis et al. 2018). The nebula is carbon- rich, with $\text{C/O} \approx 1.3$ (X.-W. Liu et al. 2001).

The distance to IC 418 is well constrained. L. Guzmán et al. (2009) determined a radio data expansion parallax distance of 1.3 ± 0.4 kpc, while C. Morisset & L. Georgiev (2009) presented a photo-ionization-model distance of 1.26 kpc. The best statistical distance is 1.3 ± 0.3 kpc from a well determined optical surface-brightness radius relation (D. J. Frew et al. 2016). The Gaia DR3 parallax is 0.73 ± 0.03 mas, yielding 1.36 ± 0.05 kpc which agrees well with these other estimates. We adopt the robust Gaia distance. The luminosity in Table A in Appendix-B is scaled from the original reference to this Gaia distance.

Our reddening estimate, from an average of 12 independent determinations of the $\text{H}\alpha/\text{H}\beta$ ratio, is $E(B - V) = 0.21 \pm 0.06$. The 6 cm radio flux over the Balmer line flux gives a reddening of $E(B - V) = 0.19$ assuming $R_V = 3.1$. A recent MUSE observation finds $E(B - V) = 0.18$ based on the Pa9 and $\text{H}\beta$ line ratio (A. Monreal-Ibero & J. R. Walsh 2022). The asymptotic reddening in this direction is $E(B - V) = 0.20$ (E. F. Schlafly & D. P. Finkbeiner 2011). All values are in good agreement. IC 418 is 600 pc above the Galaxy’s mid-plane, well above the clumpy interstellar dust layer, so agreement between the derived extinction and the asymptotic extinction is not unexpected. There is some evidence for additional internal extinction of $E(B - V) = 0.05$ in the PN’s bright rim (A. Monreal-Ibero & J. R. Walsh 2022).

³ In this paper, “ $[\text{O III}]/\text{H}\beta$ ” refers specifically to the $[\text{O III}]\lambda 5007\text{\AA}/\text{H}\beta$ ratio.

The integrated $H\alpha$ flux is $F(H\alpha) = -9.02 \pm 0.04 \text{ erg cm}^{-2} \text{ s}^{-1}$ from [D. J. Frew et al. \(2013\)](#), based on an average of two separate measurements; the de-reddened value is $I(H\alpha) = -8.81 \pm 0.05 \text{ erg cm}^{-2} \text{ s}^{-1}$. [P. Ventura et al. \(2017\)](#) argue for a low metallicity with $[O/H]$ of -0.6 but photo-ionization models of the nebula indicate solar-like values ([C. Morisset & L. Georgiev 2009](#); [M. A. Dopita et al. 2017](#)), with some evidence for depletion of Mg and Si (0.5 dex) and a large depletion of Fe (2.9 dex). We adopt the abundances of [C. Morisset & L. Georgiev \(2009\)](#).

3. THE CENTRAL STAR

The CSPN of IC 418, HD 35914, is bright and of spectral type O7f ([S. R. Heap 1977](#)), with a temperature reported as $T_{\text{eff}} = 33.5 \text{ kK}$ ([M. A. Dopita et al. 2017](#)), 36.7 kK ([C. Morisset & L. Georgiev 2009](#)) or 39 kK ([V. Escalante et al. 2012](#)), derived from photo-ionization models fitted to modern observational data. [M. A. Dopita et al. \(2017\)](#) considers the CSPN to have evolved from a fairly massive carbon star with initial mass of $2.5\text{--}3 M_{\odot}$.

Stellar magnitude measurements for HD 35914 often include contributions from the compact PN, unless explicitly corrected. [R. Ciardullo et al. \(1999\)](#) give $V = 10.23$ from HST data (after correcting for nebular contribution) while Whole Earth Telescope data from [G. Handler et al. \(1997\)](#) finds $V \simeq 9.88$ which is corrected for nebular light. Several recent photometric observations with APASS (the AAVSO Photometric All-Sky Survey) and with UCAC4 ([N. Zacharias et al. 2012](#)), give values 0.5 to 1.2 mag brighter due to inclusion of nebular light given the PN is of high surface brightness. Gaia DR3 photometry gives a B-band magnitude (from 4000 to 5000 Å) of 9.879 and R-band magnitude (from 6000 to 7500 Å) of 9.810.

The reported stellar luminosity of $L \sim 7500 \pm 1000 L_{\odot}$ places it on the constant luminosity horizontal part of the post-AGB evolutionary tracks ([M. M. Miller Bertolami 2016](#)), with a core mass of $\sim 0.57\text{--}0.62 M_{\odot}$ and an initial mass of $\sim 1.5\text{--}2.5 M_{\odot}$ based on those theoretical tracks, which is somewhat lower than the [M. A. Dopita et al. \(2017\)](#) estimates.

The CSPN shows both small-amplitude photometric and wind variations in modern observations and is the prototype of a class of cool, variable CSPN ([G. Handler et al. 1997](#); [E. Kuczwaska et al. 1997](#)). The variability is ~ 0.2 mag level peak-to-peak about the current mean value, over time scales of hours. The $B - V$ colour similarly varies by 0.05 mag. The wind velocity is $v_w = 500 \text{ km s}^{-1}$ ([C. Morisset & L. Georgiev \(2009\)](#)). The star has an enhanced helium abundance, with $\text{He}/\text{H} \approx 0.25$ ([C. Morisset & L. Georgiev 2009](#)). The nebula does not show this, indicating that stellar abundances have been modified since the ejection of the nebula.

The photographic DASCH ([J. Grindlay et al. 2009](#)) archive provides long-term photometric data for HD 35914. This shows a ~ 0.2 B-band dimming contributions from the evolving $H\beta$ and $[O \text{ III}]$ PN nebular lines within the blue band-pass. Only the 497 unflagged (higher quality) DASCH points were used but these still have considerable scatter. A linear fit quantifies the dimming rate as 0.0026 mag/year. The UCAC4 B magnitude from epoch 1985.94 is 9.405 c.f. the DASCH trend line value at the same epoch of 9.505 in reasonable agreement. The nebular contribution leaves uncertainty in the amount of stellar dimming.

The basic observed and derived properties of PN IC 418 and its CSPN are summarised in Table A in Appendix A.

4. SECULAR EVOLUTION OF THE PN IC 418

The nebula expansion has been measured directly using high-resolution radio observations ([L. Guzmán et al. 2009](#)) over 20 years. They derive a radial expansion rate of $5.8 \pm 1.5 \text{ mas yr}^{-1}$. [D. Schönberner et al. \(2018\)](#) analyse HST images over 8 year timescales and find that the nebula expands by a factor of 8×10^{-4} per year, or $5.5 \pm 0.5 \text{ mas yr}^{-1}$, in good agreement with the other measure. [D. Schönberner et al. \(2018\)](#) derive a PN age of $\sim 1185 \pm 110$ years while [C. Morisset & L. Georgiev \(2009\)](#) derive an expansion age of 1400 years. Regardless, IC 418 is among the younger PNe known. Taking a current stellar $T_{\text{eff}} = 37 \text{ kK}$, and an end-of-AGB temperature of $\sim 5 \text{ kK}$, the average heating rate of the star over the entire time interval since the star left the AGB becomes $\sim 20\text{--}30 \text{ K yr}^{-1}$. Such a rapid heating rate may cause measurable ionization structure evolution of the photo-ionized nebula over decadal timescales. This is confirmed by our investigations here.

4.1. The historical spectroscopic archive

Below we present a table of our evaluation of the historical records of optical spectroscopy of IC 418 that cover the $[O \text{ III}]$ and $H\beta$ lines, supplemented by our own observations. Full details are given in Appendix B.

Table 1. Secular change in the observed generally integrated $[\text{O III}]\lambda 5007/\text{H}\beta$ ratio with time.

Date	$[\text{O III}]/\text{H}\beta$	Line Measures	Telescope	Instrument	Detector	Reference
1893.8	0.8 ± 0.3	integrated	Lick 36" refractor	slitless spectrograph	eye	W. W. Campbell (1893)
1899	< 1.0	integrated	Lick 36" refractor	slitless spectrograph	eye	J. E. Keeler (1899)
1916.8–1917.8	0.965*	integrated	Lick 36" refractor	slitless spectrograph	photographic	W. H. Wright (1918) ¹
1938.7	1.39	integrated	Lick 36" refractor	slitless spectrograph	photographic	L. H. Aller (1941)
1940.9	1.35:	integrated	Lick 36" refractor	slitless spectrograph	photographic	A. B. Wyse (1942) ²
1952.5	1.38	integrated	24" McMath-H Obs.	interference filters	photoelectric	W. Liller (1955)
1953.8	1.33	integrated	Curtis Schmidt	slitless	photoelectric	W. Liller & L. H. Aller (1954) ³
1959.5	1.38	slit 30.4" wide	36" Pine Bluff	scanning spectrograph	photoelectric	E. R. Capriotti & C. T. Daub (1960) ⁴
1959–1963	1.27	integrated	50cm Shternberg	slitless	photographic	B. A. Vorontsov Vel'Yaminov et al. (1966)
1962.8	1.27	integrated	60"/100" Mt. Wilson	scanning spectrograph	photoelectric	C. R. O'Dell (1963) ⁵
1966.9	1.37:	slit 10" \times 45"	Lick 120" reflector	Coude spectrograph	imagetube+Ilford	L. Aller & M. Walker (1970)
1967.5 \pm 1.5	1.32	integrated	Lick Crossley 36"	aperture	photoelectric	M. Peimbert & S. Torres-Peimbert (1971)
1972–1978	1.47	2" \times 2" slots	Lick/Mt Wilson	apert.spectra 2 posns	image tube	L. H. Aller & S. J. Czyzak (1979) ⁶
1972.2 \pm 1.5	1.53	slit 8"	Hamilton Crossley 36"	sequential scanner	photoelectric	T. Barker (1978)
1973–1975	1.70	slit 4.8" \times 71.5"	CTIO	image tube spect.	IIDS	S. Torres-Peimbert & M. Peimbert (1977)
1974.5 \pm 1.5	1.53	integrated	SAAO 0.5m	interference filters	photometer	B. L. Webster (1983)
1976–1978.3	1.55	integrated	ESO 0.5/1.0m	interference filters	photoelectric	L. Kohoutek & W. Martin (1981)
1980.5	1.51	integrated	CTIO 0.9m	spectral scanner	photomultiplier	A. Gutierrez-Moreno et al. (1985)
1982.8–1983.8	1.52	integrated	ESO 1.52m	B&C spectrograph	IDS	R. Louise & G. Pascoli (1984) ⁷
1984.3–1985.3	1.64	integrated	CTIO 0.9m	interference filter	aperture phot.	R. A. Shaw & J. B. Kaler (1989) ⁸
1986.8	1.52	slit 4" \times 4"	ESO 1.52m	B&C spectrograph	CCD	Unpublished Acker ⁹
1989–1991	1.54	slit 4" EW	Brazil 1.6m	B&C spectrograph	Reticon	J. A. De Freitas Pacheco et al. (1992)
1992.2	0.86	slit 6" localised	Shane 3m	Echelle	CCD	S. Hyung et al. (1994) ¹⁰
2006.0	1.75	integrated	KPNO 0.6m	Fabry-Perot	CCD	This work [WHAM]
2008.2	1.84	integrated	3.9m AAT	SPIRAL IFU	CCD	This work [AAT]
2008.4	1.75	slit 2" EW	2.3m MSSSO	DBS	CCD	This work [MSSSO]
2014.1	1.84	integrated	ESO 8m VLT	MUSE IFU	CCD	Private communication ¹¹
2016.0	1.99	integrated	2.3m MSSSO	WiFeS IFU	CCD	M. A. Dopita et al. (2017)
2016.9	2.09	slit 2.5" EW	SAAO 1.9m	Cass Spec	CCD	This work [SAAO]
2019.8	2.01	integrated	2.3m MSSSO	WiFeS IFU	CCD	This work [MSSSO]
2024.8	1.95	slit 2.7" EW	SAAO 1.9m	SpupNic	CCD	This work [SAAO]

* The formal lower limit from reported line intensities is 0.64, however, the high blue response of the emulsion is not corrected for. This would increase this value to 1.29 but this is an upper limit. Taking the average gives 0.965

¹ The Wright spectrograms show $\text{H}\beta$ stronger than $[\text{O III}]$ but the $[\text{O III}]$ 5007/4959 ratio is reported as 1.57 c.f. the theoretically expected value of 2.98. This indicates a strong, blue sensitivity term for the photographic emulsion so the raw $[\text{O III}]/\text{H}\beta$ line ratio of 0.63 is a clear lower limit. ² The intensity ratio in the paper is an eye estimate (L. Aller & J. B. Kaler 1964) albeit done with the aid of specially prepared scale plates. Our line ratio is based on the 4959Å line as the reported 5007/4959Å ratio is unphysically large while close to the theoretical value for the other 6 PNe reported in the paper. Hence, we have assumed that the $[\text{O III}]$ 5007Å value of 230 is a typographical error and should be 130 which puts it on near par with all the other measurements in the paper; ³ From the reported sum of the two $[\text{O III}]$ lines, assuming a line ratio of 3.0; ⁴ The paper gives no observing date but the observatory only opened in 1958, so the observations were likely done in 1959 or early 1960 so we selected 1959.5; ⁵ The $[\text{O III}]/\text{H}\beta$ line ratio used is scaled from the $[\text{O III}]$ 4959Å line. Fluxes appear low for $[\text{Ne III}]$ but ok for $[\text{O II}]$. The slit was likely positioned off-centre so the result is likely less representative. ⁶ Average of two measurements given. No date is given for the observations but the instrument was in use from 1972; ⁷ Average of the central 12 values in map for $[\text{O III}]$ and $\text{H}\beta$. No dates of observation were provided but the telescope was built in 1981; ⁸ The $[\text{O III}]/\text{H}\beta$ line ratio is scaled from the $[\text{O III}]$ 4959Å line. ⁹ Unpublished spectrum from Stenholm and Acker uploaded to HASH; the $[\text{O III}]/\text{H}\beta$ ratio is measured directly from their 1-D spectra where the line peaks give 1.52 and integrated value gives 1.51; ¹⁰ Spectrum is from a localised region towards the PN edge and is not representative of the PN as a whole, it is shown as a lower limit; ¹¹ integrated ratio value determined from MUSE images of $[\text{O III}]$ 4949Å and $\text{H}\beta$ then scaled to $[\text{O III}]$ 50007Å equivalent from ESO 8m VLT MUSE IFU reduced data provided by Ana Monreal Ibero (private communication).

4.2. Spectroscopic evolution

The observed $[\text{O III}]/\text{H}\beta$ ratio is plotted against time in Fig. 1. The mostly integrated line ratios show a clear secular increase. IC 418 is compact and mildly elliptical with a major axis of 14" so even long-slit spectra with typical 2-3" slits combined with typical 2-4" seeing at the modest observing sites used implies that a reasonable fraction ($\sim 20\%$) of the full PN is sampled with slit spectra. A simple analysis of the AAT SPIRAL IFU data presented from 2008 shows that extracting virtual 2" wide slices across the PN through the centre in 15 deg radial increments only yields a variation of $\leq 7\%$ in the $[\text{O III}]/\text{H}\beta$ ratio and is in good agreement with the observed, integrated ratio.

Accepting the W. W. Campbell (1893) visual value, the $[\text{O III}]$ $\lambda 5007$ line has more than doubled in strength compared to $\text{H}\beta$ since the discovery of the PN. This clearly indicates a change in photoionization. M. A. Dopita et al. (2017) identify a shock contribution to this line of around 2.5% but this is much smaller than the observed increase.

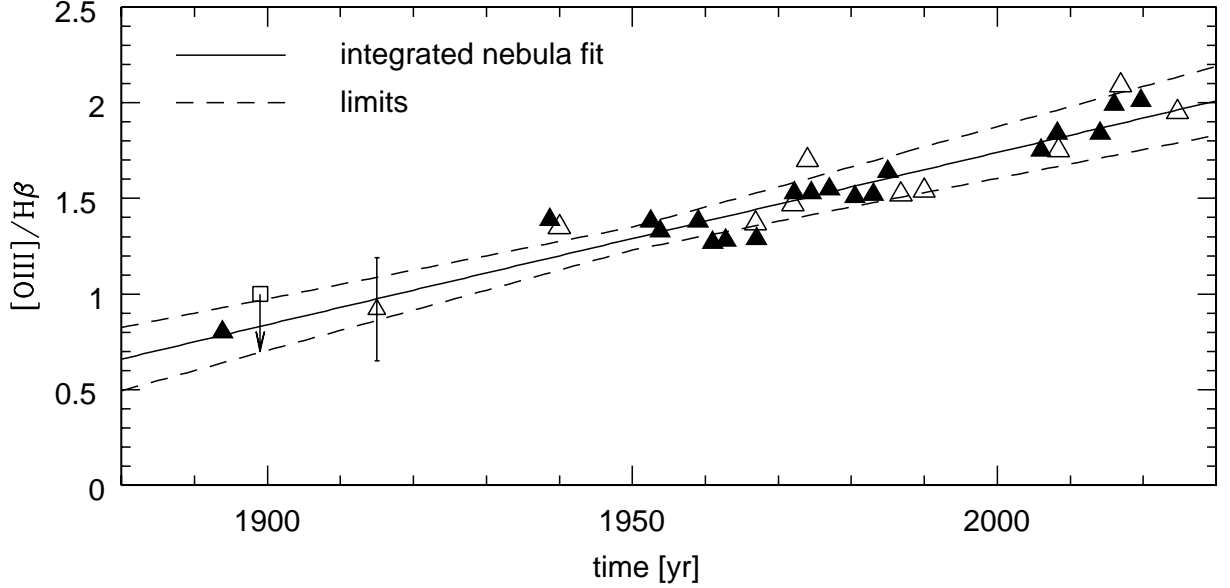


Figure 1. Observed values of $\lambda 5007/H\beta$ over a 130 year time period. The most reliable data, based on integrated flux across the full PN, are plotted as filled triangles. Open triangles refer to less reliable measurements usually derived from wide slits or apertures that do not cover all of the nebula. Open squares show limits. The off-centre data of [S. Hyung et al. \(1994\)](#) is not included. The best fit and limits are shown; this fit excludes the data from narrow slits (Table 1).

We fitted the observed line ratios with a linear fit, using the python routine `linregress` from `scipy` version 1.13.1. Selecting only the entries in Table 1 covering the entire nebula (integrated or slit wide enough to cover the full nebula: filled symbols in Fig. 1) gives:

$$F(\lambda 5007/H\beta) = (0.0090 \pm 0.0015) \times (t - 1950) + (1.29 \pm 0.06), \quad (1)$$

where t is the calendar year. The uncertainties were derived by adding normal noise to the data points, assuming $\sigma = 0.3$ for the 1893 Campbell datum and $\sigma = 0.1$ for all other data points. The 1899 Keeler and 1917 Wright data are not used in this fit (but are still plotted).

Including all data points in Table 1 apart from [L. H. Aller & S. J. Czyzak \(1979\)](#) and [S. Hyung et al. \(1994\)](#) gives:

$$F(\lambda 5007/H\beta) = (0.0089 \pm 0.0012) \times (t - 1950) + (1.30 \pm 0.05). \quad (2)$$

Without the Campbell datum, the slope becomes $(0.0091 \pm 0.001 \text{ yr}^{-1})$ in Eq. (1) and $(0.0089 \pm 0.0008 \text{ yr}^{-1})$ in Eq. (2). Thus, the Campbell value has little effect on the slope itself but dominates the uncertainty.

We conclude that the $[O \text{ III}]/H\beta$ ratio has increased approximately linearly by 0.9% per year. Continued monitoring will show whether this trend continues.

5. MODELING

The observed line ratio change is caused by the star heating up. Modeling the nebula and star is required to determine their relation. We aim not to reproduce the detailed spectrum but to model the relative changes in the $[O \text{ III}]/H\beta$ ratio. The mild (1-arcsec) angular expansion of the nebula over the historical evolution is also not considered.

A comprehensive model fit to the IC 418 PN spectrum was given by [C. Morisset & L. Georgiev \(2009\)](#) that included an extensive imaging and spectroscopic study via a pseudo 3-D photoionization code. We use a simplified 1-D version of their nebular model to investigate the dependency of the integrated $[O \text{ III}]/H\beta$ flux ratio on stellar temperature. The [C. Morisset & L. Georgiev \(2009\)](#) model combines 1-D models calculated for four different directions across the PN. This provided a good approximation while avoiding the computational complexity of full 3-D modeling. We reduced

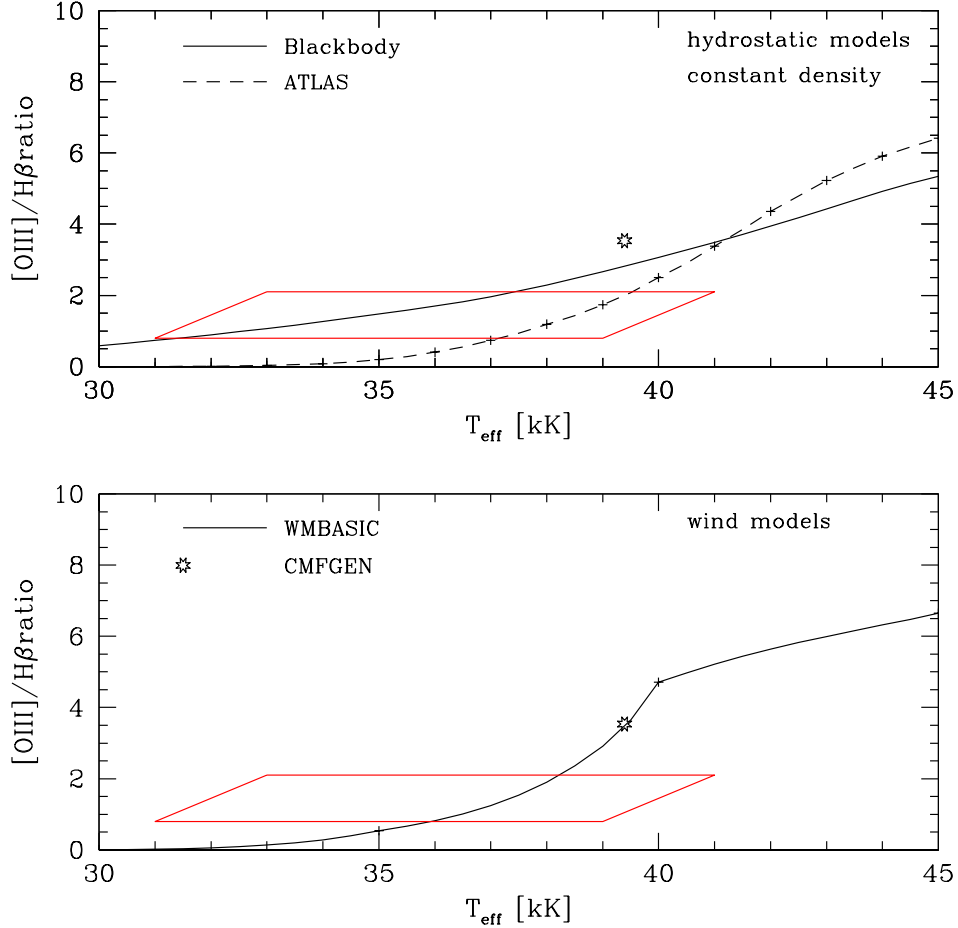


Figure 2. The predicted [O III] 5007/H β ratio as function of T_{eff} , for different stellar atmosphere models and assuming a constant density nebula. Top panel: Hydrostatic ATLAS and blackbody models. Bottom panel: WMBASIC models which include stellar winds, and the Cloudy fit for a single CMFGEN model with stellar winds from V. Escalante et al. (2012) (also shown in the top panel). The red parallelogram encompasses the range of observed [O III] 5007/H β flux ratios. The plusses indicate the stellar models which Cloudy uses for interpolation.

this to a single 1-D model, adopting the parameters of C. Morisset & L. Georgiev (2009) for the equatorial plane. For a CSPN, a blackbody function gives correct line ratios for elements with ionization potentials up to ~ 40 eV (C. Morisset & L. Georgiev 2009). The O^{++} ion requires 35.1 eV to form, and the [O III] lines have a significant dependency on the stellar atmosphere model used.

For our modeling we used nebular abundances from C. Morisset & L. Georgiev (2009) and tested the abundances of M. A. Dopita et al. (2017) but with no significant differences seen. Other parameters from C. Morisset & L. Georgiev (2009) were also adopted, but we use the Gaia DR3 distance of 1.360 ± 0.055 kpc: the inner radius, scaled to that distance, is $\log r_{\text{in}} = 16.09$ cm. A 1-D Cloudy model was computed out to the ionization radius where the electron temperature drops to $T_e = 10^3$ K. Cloudy version 23.01 was used (G. J. Ferland et al. 2013; M. Chatzikos et al. 2023) but in 1-D mode rather than the 3-D approximation used by C. Morisset & L. Georgiev (2009), equivalent to assuming a spherical nebula. This is a reasonable approximation for this mildly elliptical PN (V. Escalante et al. 2012) with an axial ratio of 0.85. Shock excitation is not included in Cloudy, but M. A. Dopita et al. (2017) find that this contributes around 2% to the [O III] emission. M. A. Guerrero et al. (2013) also find little evidence of shock emission in IC 418.

The main models used a constant density, taken as $\log n_e = 3.95$ cm $^{-3}$. Both C. Morisset & L. Georgiev (2009) and M. A. Dopita et al. (2017) adopt a double-shell model, albeit with different inner radii. We also computed models for both these distributions and found some minor differences in the integrated [O III]/H β ratios. The [O III] emissivity is dominated by the inner region, limiting the effect of the radial density distribution.

Cloudy model grids were calculated for three stellar atmosphere models provided in Cloudy: blackbody, ATLAS ODFNEW (F. Castelli & R. L. Kurucz 2003) at $\log g = 4.5$ and WMBASIC (A. W. A. Pauldrach et al. 2001) at $\log g = 4.5$. TMAP models developed for CSPN (T. Rauch et al. 2018) do not cover the temperature range for IC 418 and could not be used, while CoStar models (D. Schaerer & A. de Koter 1997) are for much higher stellar masses. The ATLAS models are for hydrostatic, plane-parallel atmospheres, with a temperature grid at steps of 1000 K. The WMBASIC models are developed for CSPN and include stellar winds. They are available at temperatures of 35, 40 and 45 kK. The value for $\log g$ for ATLAS and WMBASIC was chosen as the closest available to the $\log g = 3.55$ for IC 418 within the model set which covered the required range of stellar temperatures. All models used solar metallicity. The single CMFGEN model of V. Escalante et al. (2012) for their best fit temperature was also kindly provided to us by C. Morisset (priv. comm.). This model was also used in V. Gómez-Llanos et al. (2018).

The stellar luminosity is set at $\log L = 37.30 \text{ erg s}^{-1}$ ($5200 L_{\odot}$) for the blackbody models and at $\log L = 37.40 \text{ erg s}^{-1}$ ($6500 L_{\odot}$) for all other models. The lower L for blackbody models is because this predicts a lower temperature and therefore brighter star at visual wavelengths for the same $[\text{O III}]/\text{H}\beta$ ratio.

The stellar temperature was increased in steps of 500 K, between limits of 30 kK and 45 kK, and the ratio of $[\text{O III}]/\text{H}\beta$ over the entire nebula was obtained from the Cloudy models for each stellar temperature. The $\text{H}\beta$ flux increases by about a factor of 2 over this temperature range, mainly over the lower temperature range (A. A. Zijlstra & S. R. Pottasch 1989), but the $[\text{O III}]$ flux increases faster giving a monotonic increase in the ratio over this temperature range.

The results from the four models with constant n_e are shown in Fig. 2, separated between the hydrostatic and the wind models. The $[\text{O III}]/\text{H}\beta$ ratio increases strongly over the plotted temperature range, but the details vary between the models. For the same ratio, the derived T_{eff} can differ by $\sim 10\%$ especially at low temperatures. Blackbody models yield higher $[\text{O III}]/\text{H}\beta$ ratios at low stellar temperatures than do the other models, but at higher temperatures the others overtake them because of the effect of the ionization absorption edges, especially He^+ which has an ionization potential very close to that of O^{2+} . The CMFGEN model of V. Escalante et al. (2012) is represented by the open star symbol: it agrees with the WMBASIC model grid, but predicts an integrated $[\text{O III}]/\text{H}\beta$ ratio well above the observed value and appears to overestimate the stellar temperature.

The non-constant density distributions of C. Morisset & L. Georgiev (2009) and M. A. Dopita et al. (2017) yield minor changes. The two models differ in inner radius but this has no effect. They also have different densities. For densities below the selected value of $\log n = 3.95$ and $[\text{O III}]/\text{H}\beta < 2.5$, the ratio increases faster with stellar temperature. For higher densities, the evolution is much less density dependent. Fig. 3 shows the dependency on density, where the vertical axis gives the change in temperature required to change the $[\text{O III}]/\text{H}\beta$ ratios from unity to 2, based on Cloudy models. The lines are for constant density models; the points show the location of the density models of C. Morisset & L. Georgiev (2009) and M. A. Dopita et al. (2017), plotted at the density of their inner shell. For the former model, increasing the density by 0.05 dex does not notably change the value. We conclude that for the parameters of IC 418 the spectral evolution is little affected by the precise density, but if the density had been significantly lower, then the $[\text{O III}]/\text{H}\beta$ would have increased faster with stellar temperature. Note that the actual stellar temperatures do depend on density, even where the rate of change does not.

6. STELLAR EVOLUTION

6.1. Heating rate

To convert the observed line ratio to stellar temperature, we linearly interpolated the ratios to the Cloudy temperature grids. This was done separately for the data points and for the linear fit of Eq. 2. The results are shown in Fig. 4. The scatter reflects the uncertainty on the measured line ratio and on the temperature. Around $T_{\text{eff}} = 37 \text{ kK}$, a 5% error on the line ratio translates to a temperature uncertainty of 100 K for the model atmosphere but 300 K for a blackbody. The 1893 measurement has a larger uncertainty in the ratio, and the associated temperature is less well determined with an uncertainty of 500 K for the model atmosphere and 1000 K for the blackbody.

We fit the data to infer the temperature rate of change assuming linear evolution. Including the W. W. Campbell (1893) visual data point gives:

$$\begin{aligned}
 T_{\text{eff}} &= (34.54 \pm 0.10) \times 10^3 + (38.8 \pm 2.5) \times (t - 1950) \text{ K} \\
 &\quad \text{blackbody} \\
 T_{\text{eff}} &= (38.20 \pm 0.04) \times 10^3 + (16.1 \pm 1.0) \times (t - 1950) \text{ K}
 \end{aligned} \tag{3}$$

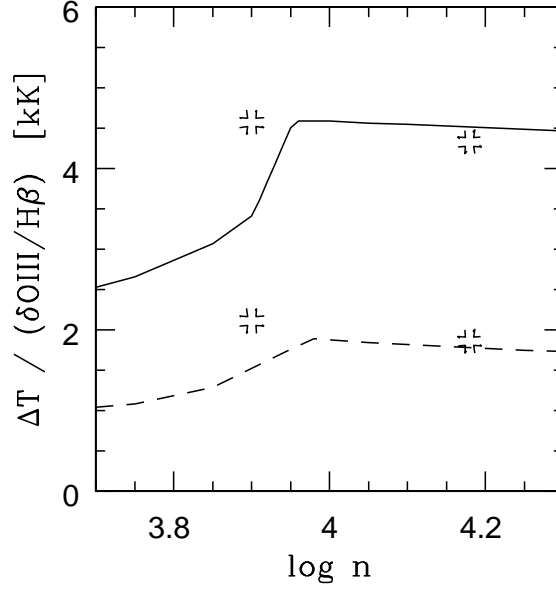


Figure 3. The change in stellar temperature needed for increasing $[\text{O III}]/\text{H}\beta$ from 1.0 to 2.0, for blackbody and ATLAS models at constant density. The drawn line is for blackbody models and the dashed line for ATLAS stellar atmospheres. The points indicate the location of the [C. Morisset & L. Georgiev \(2009\)](#) (left) and [M. A. Dopita et al. \(2017\)](#) (right) density models, shown at the density of their main inner shell, where the two upper points are for blackbody SEDs and the two lower ones for the ATLAS SEDs.

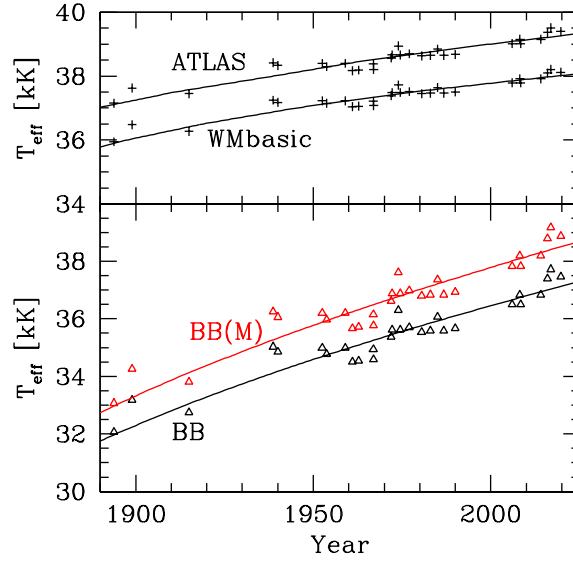


Figure 4. The derived central star temperature evolution of IC 418 based on changes in the observed $[\text{O III}]/\text{H}\beta$ line ratios. The drawn lines correspond to the linear fit of Eq. 2. The lower panel gives blackbody SEDs from the density distributions of [C. Morisset & L. Georgiev \(2009\)](#) in red - labelled BB(M) - and [M. A. Dopita et al. \(2017\)](#) - labelled BB - respectively.

$$\text{ATLAS} \tag{4}$$

where t is the calendar year. The highest value for the slope is obtained for the [C. Morisset & L. Georgiev \(2009\)](#) density distribution with a blackbody stellar atmosphere (shown in red and labeled 'BB(M)' in Fig. 4):

$$T_{\text{eff}} = (35.72 \pm 0.11) \times 10^3 + (41.7 \pm 2.7) \times (t - 1950) \text{ K}$$

(5)

The WMBASIC model is similar to the ATLAS result. Excluding the [W. W. Campbell \(1893\)](#) point reduces the slope by $\sim 5\%$, which is within the uncertainty of the fit. The slope is little affected by inclusion of the earliest data point.

The uncertainty on the conversion from $[\text{O III}]/\text{H}\beta$ evolution to a heating rate is dominated by the stellar atmosphere, which gives a range of a factor of four. The density structure causes additional uncertainty but for the parameters of IC 418 this is less than 10%. Based on the explored parameter range, the highest heating rate is 41.7 K/yr, based on the density distribution of [C. Morisset & L. Georgiev \(2009\)](#) and a blackbody atmosphere. The ATLAS stellar atmospheres give a heating rates of 16.1 ± 1.0 K/yr and WMBASIC 15.2 ± 1.0 K/yr.

6.2. Stellar mass

The heating rate is a strong function of central star mass ([K. Gesicki et al. 2014](#)). Recent post-AGB models of [M. M. Miller Bertolami \(2016\)](#) ($Z = 0.01$, H-burning) predict heating rates ranging from 2 to 180 K/yr at stellar temperatures of 30–40 kK, for central star masses between 0.53 and 0.62 M_{\odot} . These heating rates cover two orders of magnitude. The luminosities vary only by a factor of ~ 3 over this mass range. This makes the heating rate by far the best determinant of stellar mass.

The derived model-dependent heating rates of 10–40 K/yr corresponds to stellar masses of 0.560–0.583 M_{\odot} , where the stellar atmosphere models are at the low end and the blackbody models at the high end of the mass range. Both lower and higher masses can be excluded at good confidence. The indicated mass range is also consistent with the stellar luminosity derived here, of $L = 5200\text{--}6500 L_{\odot}$.

The stellar mass is related to the initial stellar mass by the initial-final mass relation. Using the initial masses in the models of [M. M. Miller Bertolami \(2016\)](#), the range corresponds to main-sequence masses of $M_i = 1.25\text{--}1.55 M_{\odot}$.

An interesting aside is that the initial-final mass relations show a bump around initial masses of 1.5–1.9 M_{\odot} ([P. Marigo et al. 2020](#)) which is apparent in the [M. M. Miller Bertolami \(2016\)](#) models. The heating rates do not show this and appear to correlate better with the initial masses than do the final masses.

7. DISCUSSION AND CONCLUSIONS

The heating rate provide a narrow mass range for IC 418's CSPN. The nebula is carbon rich ([X.-W. Liu et al. 2001](#)). This provides another constraint as low-mass stars do not dredge-up sufficient carbon to achieve $\text{C/O} > 1$. [P. Marigo et al. \(2020\)](#) find a minimum mass of $M_i > 1.65 M_{\odot}$ for stars to become carbon stars at solar metallicity, with $\text{C/O} = 1.3$ (the value for IC 418 from [X.-W. Liu et al. \(2001\)](#)) reached for $M_i = 1.8\text{--}1.9 M_{\odot}$. These values are outside the mass range derived from the heating rate. In contrast, [N. R. Rees et al. \(2024\)](#) find a minimum initial mass for carbon star formation of $M_i = 1.5\text{--}1.75 M_{\odot}$, and [A. I. Karakas & M. Lugaro \(2016\)](#) derived $1.4\text{--}2 M_{\odot}$ which does overlap with the mass range derived here but only for blackbody models. The stellar atmosphere models, which may be more realistic, give masses that are below the carbon-star range. This important contradiction indicates that some aspects of the AGB-PN evolution may be uncertain.

Given the complexity of this evolutionary phase, it is difficult to pin-point one aspect that might be the issue. A possibility is in the stellar atmosphere models which are not optimised for post-AGB stars; it is important to compute new models which include a wind, as is present in IC 418 ([C. Morisset & L. Georgiev 2009](#)). Using other ions than O^{++} may reduce the sensitivity to these models.

Alternatively, the post-AGB stellar evolution models may overestimate heating rates. Instantaneous heating rates derived here are compatible with those derived from the nebula's kinematic age (~ 25 K/yr), leaving the possibility that post-AGB models evolve too fast. They also use grey atmospheres for the calculations rather than full atmosphere models, so the model temperatures may deviate from the observed ones. Finally, the initial-final mass relations may overstate the final masses, as possibly indicated for NGC 3132 ([O. De Marco et al. 2022](#)) and cluster PNe ([V. Fragkou et al. 2025](#)).

In conclusion, we have, for the first time, shown robust, direct, secular evolution of a CSPN over an unprecedented 130 year time period. This provides an important new tracer for the evolution of post-AGB stars. Implications are that at solar metallicity the lower mass cutoff for carbon-star formation may need further consideration.

ACKNOWLEDGEMENTS

Dr. David Frew initiated this project and carried out research across Sections 1–4, but unfortunately has left academia. He deserves special mention: the authors gratefully acknowledge his crucial role.

Q.A.P. thanks the Hong Kong Research Grants Council for GRF research support under grants 17304024, 17326116 and 17300417. A.A.Z. thanks the Hung Hing Ying Foundation for a visiting HKU professorship and acknowledges UK STFC funding under grants ST/T000414/1 and ST/X001229/1. A.A.Z. also acknowledges support from the Royal Society through grant IES/R3/233287 and from the University of Macquarie. This work made use of the University of Hong Kong/Australian Astronomical Observatory/Strasbourg Observatory H-alpha Planetary Nebula (HASH PN) database, hosted by the Laboratory for Space Research at the University of Hong Kong. Use was made of the TMAW tool (<http://astro.uni-tuebingen.de/TMAW>), constructed as part of the activities of the German Astrophysical Virtual Observatory. The authors thank Dr. Andreas Ritter for assistance with AAT SPIRAL, ANU 2.3m WIFES IFU and SAAO 2024 SpuPNIC data of IC 418. We thank Ana Monreal Ibero for the ESO 8m VLT MUSE IFU data point from 2014, and Christophe Morisset for providing us with the CMFGEN model for the central star.

REFERENCES

- Acker, A., Marcout, J., Ochsenbein, F., et al. 1992, The Strasbourg-ESO Catalogue of Galactic Planetary Nebulae. Parts I, II. (European Southern Observatory, Garching (Germany))
- Ali, A., Amer, M. A., Dopita, M. A., Vogt, F. P. A., & Basurah, H. M. 2015, *A&A*, 583, A83, doi: [10.1051/0004-6361/201526223](https://doi.org/10.1051/0004-6361/201526223)
- Aller, L., & Kaler, J. B. 1964, *ApJ*, 140, 936, doi: [10.1086/147996](https://doi.org/10.1086/147996)
- Aller, L., & Walker, M. 1970, *ApJ*, 161, 917, doi: [10.1086/150594](https://doi.org/10.1086/150594)
- Aller, L. H. 1941, *ApJ*, 93, 236, doi: [10.1086/144260](https://doi.org/10.1086/144260)
- Aller, L. H., & Czyzak, S. J. 1979, *Ap&SS*, 62, 397, doi: [10.1007/BF00645478](https://doi.org/10.1007/BF00645478)
- Aller, L. H., & Liller, W. 1966, *MNRAS*, 132, 337, doi: [10.1093/mnras/132.2.337](https://doi.org/10.1093/mnras/132.2.337)
- Arhipova, V. P., Kostyakova, E. B., Burlak, M. A., Esipov, V. F., & Ikonnikova, N. P. 2014, *Astronomy Reports*, 58, 702, doi: [10.1134/S1063772914100023](https://doi.org/10.1134/S1063772914100023)
- Bandyopadhyay, R., Das, R., Parthasarathy, M., & Kar, S. 2023, *MNRAS*, 524, 1547, doi: [10.1093/mnras/stad1897](https://doi.org/10.1093/mnras/stad1897)
- Barker, T. 1978, *ApJ*, 219, 914, doi: [10.1086/155854](https://doi.org/10.1086/155854)
- Barker, T. 1979, *ApJ*, 227, 863, doi: [10.1086/156796](https://doi.org/10.1086/156796)
- Bloecker, T. 1995, *A&A*, 299, 755
- Boeshaar, G. O. 1974, *ApJ*, 187, 283, doi: [10.1086/152627](https://doi.org/10.1086/152627)
- Campbell, W. W. 1893, *PASP*, 5, 207, doi: [10.1086/120677](https://doi.org/10.1086/120677)
- Campbell, W. W. 1894, *Astronomy and Astro-Physics* (formerly *The Sidereal Messenger*), 13, 384,494
- Capriotti, E. R., & Daub, C. T. 1960, *ApJ*, 132, 677, doi: [10.1086/146972](https://doi.org/10.1086/146972)
- Castelli, F., & Kurucz, R. L. 2003, in *Modelling of Stellar Atmospheres*, ed. N. Piskunov, W. W. Weiss, & D. F. Gray, Vol. 210, A20, doi: [10.48550/arXiv.astro-ph/0405087](https://doi.org/10.48550/arXiv.astro-ph/0405087)
- Cerrigone, L., Umana, G., Trigilio, C., et al. 2017, *MNRAS*, 468, 3450, doi: [10.1093/mnras/stx690](https://doi.org/10.1093/mnras/stx690)
- Chatzikos, M., Bianchi, S., Camilloni, F., et al. 2023, *RMxAA*, 59, 327, doi: [10.22201/ia.01851101p.2023.59.02.12](https://doi.org/10.22201/ia.01851101p.2023.59.02.12)
- Ciardullo, R., Bond, H. E., Sipior, M. S., et al. 1999, *AJ*, 118, 488, doi: [10.1086/300940](https://doi.org/10.1086/300940)
- CIE. 1951, *Commission Internationale de l'Eclairage Proceedings*, Vol. 1, Sec 4; Vol 3, p. 37, Tech. rep., Bureau Central de la CIE, Paris
- Cummings, J. D., Kalirai, J. S., Tremblay, P. E., Ramirez-Ruiz, E., & Choi, J. 2018, *ApJ*, 866, 21, doi: [10.3847/1538-4357/aadfd6](https://doi.org/10.3847/1538-4357/aadfd6)
- De Freitas Pacheco, J. A., Maciel, W. J., & Costa, R. D. D. 1992, *A&A*, 261, 579
- De Marco, O., Akashi, M., Akras, S., et al. 2022, *Nature Astronomy*, 6, 1421, doi: [10.1038/s41550-022-01845-2](https://doi.org/10.1038/s41550-022-01845-2)
- Díaz-Luis, J. J., García-Hernández, D. A., Manchado, A., et al. 2018, *AJ*, 155, 105, doi: [10.3847/1538-3881/aaa75c](https://doi.org/10.3847/1538-3881/aaa75c)
- Dopita, M. A., Ali, A., Sutherland, R. S., Nicholls, D. C., & Amer, M. A. 2017, *MNRAS*, 470, 839, doi: [10.1093/mnras/stx1166](https://doi.org/10.1093/mnras/stx1166)
- Escalante, V., Morisset, C., & Georgiev, L. 2012, *MNRAS*, 426, 2318, doi: [10.1111/j.1365-2966.2012.21862.x](https://doi.org/10.1111/j.1365-2966.2012.21862.x)
- Feibelman, W. A., Aller, L. H., & Hyung, S. 1992, *PASP*, 104, 339, doi: [10.1086/133003](https://doi.org/10.1086/133003)
- Ferland, G. J., Porter, R. L., van Hoof, P. A. M., et al. 2013, *RMxAA*, 49, 137. <https://arxiv.org/abs/1302.4485>
- Fragkou, V., Vázquez, R., Parker, Q. A., Gonçalves, D. R., & Lomelí-Núñez, L. 2025, *A&A*, 696, A146, doi: [10.1051/0004-6361/202453031](https://doi.org/10.1051/0004-6361/202453031)
- Frew, D. J., Bojičić, I. S., & Parker, Q. A. 2013, *MNRAS*, 431, 2, doi: [10.1093/mnras/sts393](https://doi.org/10.1093/mnras/sts393)

- Frew, D. J., Parker, Q. A., & Bojićić, I. S. 2016, *MNRAS*, 455, 1459, doi: [10.1093/mnras/stv1516](https://doi.org/10.1093/mnras/stv1516)
- Gesicki, K., & Zijlstra, A. A. 2007, *A&A*, 467, L29, doi: [10.1051/0004-6361:20077250](https://doi.org/10.1051/0004-6361:20077250)
- Gesicki, K., Zijlstra, A. A., Hajduk, M., & Szyszka, C. 2014, *A&A*, 566, A48, doi: [10.1051/0004-6361/201118391](https://doi.org/10.1051/0004-6361/201118391)
- Gómez-Llanos, V., Morisset, C., Szczerba, R., García-Hernández, D. A., & García-Lario, P. 2018, *A&A*, 617, A85, doi: [10.1051/0004-6361/201731707](https://doi.org/10.1051/0004-6361/201731707)
- Gómez-Muñoz, M. A., García-Hernández, D. A., Manchado, A., Barzaga, R., & Huertas-Roldán, T. 2024, *MNRAS*, 528, 2871, doi: [10.1093/mnras/stae218](https://doi.org/10.1093/mnras/stae218)
- Griffith, M. R., Wright, A. E., Burke, B. F., & Ekers, R. D. 1994, *ApJS*, 90, 179, doi: [10.1086/191863](https://doi.org/10.1086/191863)
- Grindlay, J., Tang, S., Simcoe, R., et al. 2009, in *Astronomical Society of the Pacific Conference Series*, Vol. 410, *Preserving Astronomy's Photographic Legacy: Current State and the Future of North American Astronomical Plates*, ed. W. Osborn & L. Robbins, 101
- Guerrero, M. A., Toalá, J. A., Medina, J. J., et al. 2013, *A&A*, 557, A121, doi: [10.1051/0004-6361/201321786](https://doi.org/10.1051/0004-6361/201321786)
- Gutierrez-Moreno, A., Moreno, H., & Cortes, G. 1985, *PASP*, 97, 397, doi: [10.1086/131551](https://doi.org/10.1086/131551)
- Guzmán, L., Loinard, L., Gómez, Y., & Morisset, C. 2009, *AJ*, 138, 46, doi: [10.1088/0004-6256/138/1/46](https://doi.org/10.1088/0004-6256/138/1/46)
- Hajduk, M., van Hoof, P. A. M., Gesicki, K., et al. 2014, *A&A*, 567, A15, doi: [10.1051/0004-6361/201322742](https://doi.org/10.1051/0004-6361/201322742)
- Hajduk, M., van Hoof, P. A. M., & Zijlstra, A. A. 2015, *A&A*, 573, A65, doi: [10.1051/0004-6361/201423629](https://doi.org/10.1051/0004-6361/201423629)
- Handler, G., Mendez, R. H., Medupe, R., et al. 1997, *A&A*, 320, 125
- Heap, S. R. 1977, *ApJ*, 215, 609, doi: [10.1086/155395](https://doi.org/10.1086/155395)
- Höfner, S., & Olofsson, H. 2018, *A&ARv*, 26, 1, doi: [10.1007/s00159-017-0106-5](https://doi.org/10.1007/s00159-017-0106-5)
- Huggins, W., & Miller, W. A. 1864, *Philosophical Transactions of the Royal Society of London Series I*, 154, 437
- Hyung, S., Aller, L. H., & Feibelman, W. A. 1994, *PASP*, 106, 745, doi: [10.1086/133438](https://doi.org/10.1086/133438)
- Karakas, A. I., & Lugaro, M. 2016, *ApJ*, 825, 26, doi: [10.3847/0004-637X/825/1/26](https://doi.org/10.3847/0004-637X/825/1/26)
- Keeler, J. E. 1899, *ApJ*, 9, 133, doi: [10.1086/140562](https://doi.org/10.1086/140562)
- Kohoutek, L., & Martin, W. 1981, *A&AS*, 44, 325
- Kostyakova, E. B., & Arhipova, V. P. 2009, *Astronomy Reports*, 53, 1155, doi: [10.1134/S1063772909120087](https://doi.org/10.1134/S1063772909120087)
- Krtićka, J., Kubát, J., & Krtićková, I. 2020, *A&A*, 635, A173, doi: [10.1051/0004-6361/201937150](https://doi.org/10.1051/0004-6361/201937150)
- Kuczańska, E., Włodarczyk, K., & Zola, S. 1997, *A&A*, 319, 161
- Kwitter, K. B., & Henry, R. B. C. 2022, *PASP*, 134, 022001, doi: [10.1088/1538-3873/ac32b1](https://doi.org/10.1088/1538-3873/ac32b1)
- Lesser, M. 2015, *PASP*, 127, 1097, doi: [10.1086/684054](https://doi.org/10.1086/684054)
- Liller, W. 1955, *ApJ*, 122, 240, doi: [10.1086/146082](https://doi.org/10.1086/146082)
- Liller, W., & Aller, L. H. 1954, *ApJ*, 120, 48, doi: [10.1086/145880](https://doi.org/10.1086/145880)
- Liu, X.-W., Barlow, M. J., Cohen, M., et al. 2001, *MNRAS*, 323, 343, doi: [10.1046/j.1365-8711.2001.04180.x](https://doi.org/10.1046/j.1365-8711.2001.04180.x)
- Louise, R., & Pascoli, G. 1984, *A&A*, 139, 529
- Marigo, P., Cummings, J. D., Curtis, J. L., et al. 2020, *Nature Astronomy*, 4, 1102, doi: [10.1038/s41550-020-1132-1](https://doi.org/10.1038/s41550-020-1132-1)
- Miller Bertolami, M. M. 2016, *A&A*, 588, A25, doi: [10.1051/0004-6361/201526577](https://doi.org/10.1051/0004-6361/201526577)
- Monreal-Ibero, A., & Walsh, J. R. 2022, *Galaxies*, 10, 18, doi: [10.3390/galaxies10010018](https://doi.org/10.3390/galaxies10010018)
- Morisset, C., & Georgiev, L. 2009, *A&A*, 507, 1517, doi: [10.1051/0004-6361/200912413](https://doi.org/10.1051/0004-6361/200912413)
- O'Dell, C. R. 1963, *ApJ*, 138, 1018, doi: [10.1086/147703](https://doi.org/10.1086/147703)
- Osterbrock, D., & Stockhausen, R. 1961, *ApJ*, 133, 2, doi: [10.1086/146998](https://doi.org/10.1086/146998)
- Otsuka, M., Kemper, F., Cami, J., Peeters, E., & Bernard-Salas, J. 2014, *MNRAS*, 437, 2577, doi: [10.1093/mnras/stt2070](https://doi.org/10.1093/mnras/stt2070)
- Parker, Q. A. 2022, *Frontiers in Astronomy and Space Sciences*, 9, 895287, doi: [10.3389/fspas.2022.895287](https://doi.org/10.3389/fspas.2022.895287)
- Pauldrach, A. W. A., Hoffmann, T. L., & Lennon, M. 2001, *A&A*, 375, 161, doi: [10.1051/0004-6361:20010805](https://doi.org/10.1051/0004-6361:20010805)
- Peimbert, M., & Torres-Peimbert, S. 1971, *Boletín de los Observatorios Tonantzintla y Tacubaya*, 6, 21
- Pickering, E. C., & Fleming, W. 1891, *Astronomische Nachrichten*, 128, 11, doi: [10.1002/asna.18911280104](https://doi.org/10.1002/asna.18911280104)
- Ramos-Larios, G., Vázquez, R., Guerrero, M. A., et al. 2012, *MNRAS*, 423, 3753, doi: [10.1111/j.1365-2966.2012.21165.x](https://doi.org/10.1111/j.1365-2966.2012.21165.x)
- Rauch, T., Demleitner, M., Hoyer, D., & Werner, K. 2018, *MNRAS*, 475, 3896, doi: [10.1093/mnras/sty056](https://doi.org/10.1093/mnras/sty056)
- Rees, N. R., Izzard, R. G., & Karakas, A. I. 2024, *MNRAS*, 527, 9643, doi: [10.1093/mnras/stad3690](https://doi.org/10.1093/mnras/stad3690)
- Reindl, N., Rauch, T., Miller Bertolami, M. M., Todt, H., & Werner, K. 2017, *MNRAS*, 464, L51, doi: [10.1093/mnrasl/slw175](https://doi.org/10.1093/mnrasl/slw175)
- Sánchez Contreras, C., Báez-Rubio, A., Alcolea, J., Bujarrabal, V., & Martín-Pintado, J. 2017, *A&A*, 603, A67, doi: [10.1051/0004-6361/201730385](https://doi.org/10.1051/0004-6361/201730385)
- Schaerer, D., & de Koter, A. 1997, *A&A*, 322, 598, doi: [10.48550/arXiv.astro-ph/9611068](https://doi.org/10.48550/arXiv.astro-ph/9611068)
- Schlafly, E. F., & Finkbeiner, D. P. 2011, *ApJ*, 737, 103, doi: [10.1088/0004-637X/737/2/103](https://doi.org/10.1088/0004-637X/737/2/103)

- Schönberner, D., Balick, B., & Jacob, R. 2018, *A&A*, 609, A126, doi: [10.1051/0004-6361/201731788](https://doi.org/10.1051/0004-6361/201731788)
- Shaw, R. A., & Kaler, J. B. 1989, *ApJS*, 69, 495, doi: [10.1086/191320](https://doi.org/10.1086/191320)
- Smith, B. A. 1976, in *Charge-Coupled Device Technology and Applications*, 135–138
- Taylor, A. R., Gussie, G. T., & Goss, W. M. 1989, *ApJ*, 340, 932, doi: [10.1086/167447](https://doi.org/10.1086/167447)
- Torres-Peimbert, S., & Peimbert, M. 1977, *RMxAA*, 2, 181
- Ventura, P., Stanghellini, L., Dell’Agli, F., & García-Hernández, D. A. 2017, *MNRAS*, 471, 4648, doi: [10.1093/mnras/stx1907](https://doi.org/10.1093/mnras/stx1907)
- Vorontsov Vel’Yaminov, B. A., Kostyakova, E. B., Dokuchaeva, O. D., & Arkhipova, V. P. 1966, *Soviet Ast.*, 9, 564
- Webster, B. L. 1983, *PASP*, 95, 610, doi: [10.1086/131226](https://doi.org/10.1086/131226)
- Wright, W. H. 1918, *Publications of Lick Observatory*, 13, 191
- Wyse, A. B. 1942, *ApJ*, 95, 356, doi: [10.1086/144409](https://doi.org/10.1086/144409)
- Zacharias, N., Finch, C. T., Girard, T. M., et al. 2012, *VizieR Online Data Catalog: UCAC4 Catalogue* (Zacharias+, 2012),, *VizieR On-line Data Catalog: I/322A*. Originally published in: 2012yCat.1322....0Z; 2013AJ....145...44Z CDS, Strasbourg
- Zijlstra, A. A., & Pottasch, S. R. 1989, *A&A*, 216, 245
- Zijlstra, A. A., van Hoof, P. A. M., & Perley, R. A. 2008, *ApJ*, 681, 1296, doi: [10.1086/588778](https://doi.org/10.1086/588778)

APPENDIX

A. BASIC PROPERTIES OF PN IC 418 AND ITS CENTRAL STAR HD 35914 FROM THE LITERATURE OR THIS WORK

Name	IC 418	HASH ID #752 Q. A. Parker (2022)
RA (J2000)	05 27 28.21	
Dec (J2000)	−12 41 50.3	
l	215.212	
b	−24.284	
Distance	1.36 ± 0.055 kpc	Gaia DR3
<i>Planetary Nebula</i>		
Dimensions (″)	14×12	D. J. Frew et al. (2016)
$\log F(\text{H}\alpha)$	-9.02 ± 0.04	D. J. Frew et al. (2013)
$\log F(\text{H}\beta)$	-9.58 ± 0.05	A. Acker et al. (1992)
$F_{6\text{cm}}$	1710 mJy	M. R. Griffith et al. (1994)
c	0.31 ± 0.08	this work
$E(B - V)$	0.21 ± 0.06	this work
$\langle n_e \rangle$	9000 cm^{-3}	M. A. Dopita et al. (2017)
T_e	9000 K	C. Morisset & L. Georgiev (2009)
Inner radius	$1.23 \times 10^{16} \text{ cm}$	C. Morisset & L. Georgiev (2009)
Outer radius	$1.4 \times 10^{17} \text{ cm}$	C. Morisset & L. Georgiev (2009)
	0.045 pc	
Kinematic age	$\sim 1185 \pm 110 \text{ yr}$	D. Schönberner et al. (2018)
	$\sim 1400 \text{ yrs}$	C. Morisset & L. Georgiev (2009)
v_{exp}	30 km/s	L. Guzmán et al. (2009)
<i>Central star*</i>		
V	10.23	R. Ciardullo et al. (1999, HST)
I_c	10.22	R. Ciardullo et al. (1999)
T_{eff}	36.7 kK	C. Morisset & L. Georgiev (2009)
L	$7500 L_{\odot}$	C. Morisset & L. Georgiev (2009), J. Krtićka et al. (2020), M. A. Gómez-Muñoz et al. (2024)
$\log g$	3.55	C. Morisset & L. Georgiev (2009)
Spectral type	O7f	(S. R. Heap 1977)
Wind velocity v_w	500 km s^{-1}	(C. Morisset & L. Georgiev 2009)
M_{core}	$0.560\text{--}0.583 M_{\odot}$	this work
$M_{\text{progenitor}}$	$1.25\text{--}1.55 M_{\odot}$	this work

*nebular contribution removed from photometric estimates of the star c.f. tabulated values in SIMBAD where $V=9.01$ from UCAC4 data of the system N. Zacharias et al. (2012).

B. THE HISTORICAL SPECTROSCOPIC ARCHIVE

To assess evidence for secular evolution in line intensity ratios and of the diagnostic $[\text{O III}]/\text{H}\beta$ ratio, it is essential to carefully evaluate the integrity of all available spectral observations reported for IC 418 over the 130 year time period of available data. This is important given the wide range of technologies employed where variables include: observatory sites and telescopes (refracting and reflecting), spectrographs (slits, slitless, prisms, grisms, gratings, IFUs and Fabry-Perot etalons) and detectors (eye, photographic plates, image tubes and CCDs). We have carefully examined all original publications and, where justified, applied corrections based on subsequent knowledge (such as the now known theoretical line ratio for the $[\text{O III}]$ doublet). This was objectively done to provide the best possible values for this study. The results are summarised in Table 1 in the main body of the paper, with particular attention paid to the observations prior to the advent of CCDs.

IC 418 was discovered in 1891 by Williamina Fleming at Harvard Observatory (E. C. Pickering & W. Fleming 1891). The $[\text{O III}]/\text{H}\beta$ ratio was noted as being notably low compared to other PNe known at the time. She stated that "the visual spectrum differs strikingly from that of other planetary nebulae". In 1891 IC 418 would have been $\sim 0.7''$ (5%) smaller than it is now based on the modern determined expansion rates (L. Guzmán et al. 2009; D. Schönberner et al. 2018).

W. W. Campbell (1893, 1894) appears to have made the first recorded spectral observation on Nov 2, 1893, with a visual spectroscope with a wide slit to include all the PN. He noticed that the two “nebulium” lines N1 (4949Å) and N2 (5007Å) (unidentified then, but now known to be the [O III] lines) were slightly less extended and more centrally condensed than H β . He measured a brightness ratio by eye using a dark wedge and blocking off an increasing fraction of the light for one line until the brightness appeared equal. This showed the brightness of the H β line to lie midway between the two [O III] doublet lines. He quotes a brightness ratio for $\lambda 5007\text{:H}\beta\text{:}\lambda 4959$ of 10:7:3. Multiplying these surface brightness values by the respective image sizes (which he reports as 11 and 14”) gives an intensity ratio of $\lambda 5007\text{:H}\beta$ of 0.9 ± 0.3 . We correct this for the scotopic spectral response of the human eye using the CIE 1951 curve CIE (1951) which at H β is 88% that at [O III] 5007Å. The corrected ratio is $[\text{O III}]/\text{H}\beta = 0.8 \pm 0.3$.

The fact that the [[O III] image is more ‘compact’ than H β was confirmed by J. E. Keeler (1899) but Keeler does not provide intensity ratios. Based on the perceived size difference we report his [O III]/H β value as < 1 .

Subsequent observations were made with photographic plates, image tube scanners or photoelectric photometers, sometimes in combination, until the advent of CCDs from 1976 onwards, e.g. (B. A. Smith 1976; M. Lesser 2015). The earliest photographic observation appears to be from W. H. Wright (1918) who obtained blue spectra from a quartz slitless spectrograph that appeared to also show H β stronger than [O III], again implying that $[\text{O III}]\lambda 5007\text{:H}\beta < 1$. However, there is clearly some strong non-linearity in the blue response of these early Eastman Kodak “Seed 23” glass plate emulsions as a function of wavelength. This is apparent from the reported relative intensities of the two “nebulium” lines (i.e. [O III]5007/4959Å) are given as 33:22, a ratio of only 1.5 when this ratio should theoretically be 2.98. The formal reported $\lambda 5007\text{:H}\beta$ relative intensity ratio is 33:51 (ratio 0.64) which is a clear lower limit. Simply correcting the H β line for the observed to the theoretical [O III]5007/4959Å ratio gives a $\lambda 5007\text{:H}\beta$ ratio of 1.29. This is likely an over-correction so we regard this as the upper limit. We adopt a mid-point value of 0.965 ± 0.3 as the best estimate from these data.

No spectra were published for the next 20 years until results from a careful analysis of a quartz slitless spectrograph photographic plate spectra from the Lick Observatory Crossley 36-inch reflector in 1938 L. H. Aller (1941). Here the [O III] line was reported brighter than H β with a formal reported ratio of 1.39. There is some confidence in this value as the reported relative intensities from the [O III] 5007/4959Å for IC 418, and indeed for 6 other PNe in his paper, have values close to the theoretical value of 3.0 with an average for all the PNe of 2.83 with $\sigma = 0.09$. Subsequent measurements found $[\text{O III}]/\text{H}\beta \approx 1.4$. All post year 2000 measurements continue to give increasing ratios that are now reported in excess of 1.7 and up to ~ 2.0 .

The most reliable [O III]/H β ratios collected and assessed are given in Table 1. The exact observation time is not always known, and some papers give a range of dates. This is reflected in the uncertainties on years given in the table. Some measurements did not integrate along the slit but present ratios from the PN’s centre where [O III] is stronger due to ionisation stratification (e.g. S. Torres-Peimbert & M. Peimbert 1977). The deep spectrum of S. Hyung et al. (1994) was centred on the outer ring where [O III] is weak. These measurements are listed but are excluded from the analysis. Some papers use earlier observations to supplement or calibrate their data and so cannot be used as independent measurements (e.g. D. Osterbrock & R. Stockhausen 1961; L. Aller & M. Walker 1970; G. O. Boeshaar 1974). Hence these estimates were excluded from our analysis.

Measurements derived from photographic plates are more uncertain due to calibration difficulties, especially as the [O III] 4959 and 5007Å lines fall at the far red end of the sensitivity curve for the old blue emulsions. This affects the L. H. Aller (1941) results, who observed IC 418 with the Crossley reflector and slitless quartz spectrograph at Lick Observatory in September 1938, among a group of about a dozen PN. Five IC 418 plates were taken with the deep blue Wratten 50 filter and Eastman 33 emulsion of the so called “photographic region” with exposures of 5 to 31 minutes. The Wratten filter has very low transmission redward of 5000Å (Wratten filters 4th edition, Eastman Kodak Co. 1920) but both [O III] 4959 and 5007Å line intensities were recorded for all PNe in the sample. The 5007/4950 ratios from the reported line intensities range from 2.69 (NGC 6572) to 2.96 (NGC 6826), c.f. the theoretical ratio of 3.0. The value for IC 418 is 2.78 from the reported intensities of 13.9 and 5.0 – the weakest for all PNe in the sample.

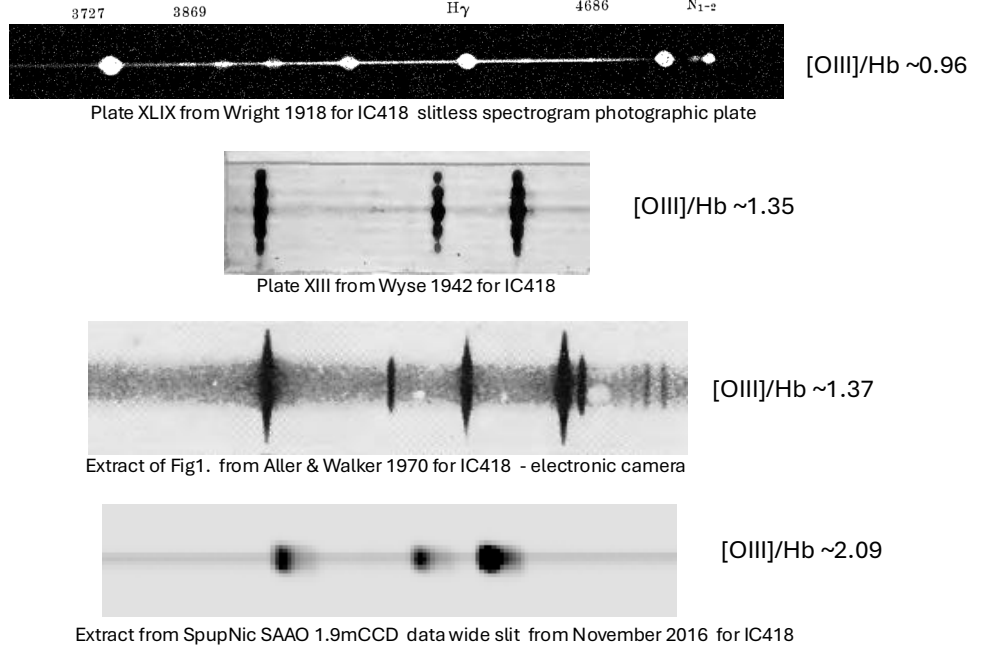


Figure 5. Selected historical examples of 2-D spectra of IC418 covering the H β and [O III] region from years 1918 to 2016. The change in the [O III] to H β ratio is clear, notwithstanding corrections for emulsion sensitivity for the 1918 and 1942 photographic plates. From top to bottom we show a slitless IC418 spectrum given in [W. H. Wright \(1918\)](#); a slit spectrum from [A. B. Wyse \(1942\)](#); an electronic camera spectrum from [L. Aller & M. Walker \(1970\)](#) and finally a 2-D extract from the CCD SpupNic image from the SAAO 1.9m taken by the second author in November 2016 all together with the estimated [O III] to H β ratios.